Journal of Applied Sciences and Nanotechnology

Journal homepage: jasn.uotechnology.edu.iq

Electrochemical Aspect of Protection Reinforced Steel Bar by Copper Coating via Modified Rolling Technique

[1]Sana Hameed, [2]Rana Afif Anaee*, [3]Ahmed Al-Ghaban, [4]Hussain Yousif

[1]Iraqi Ministry of Transport, Iraq
[2]Nanotechnology and Advanced Materials Research Center, University of Technology, Iraq
[3]College of Materials Engineering, University of Technology-Iraq, Iraq
[4]State Company for Steel Industries, Ministry of Industry and Minerals, Iraq

A R T I C L E I N F O

Article history:
Received: March, 20, 2025
Accepted: September, 20, 2025
Available online: December, 10, 2025

Keywords:
Steel bar,
Copper,
Corrosion,
Coating,
Hot Rolling

Corresponding Author:
Rana Afif Anaee
dr.rana_afif@yahoo.com

A B S T R A C T

This study investigates the corrosion resistance of copper-coated reinforcing steel bars embedded in concrete and exposed to a simulated marine environment for 28, 56, and 90 days. At temperatures of (298, 308, and 318 Kelvin). A novel thermal spray technique was integrated into the hot rolling process to deposit copper powder onto heated steel bars. The coated bars were characterized using X-ray diffraction (XRD), scanning electron microscopy with energy-dispersive spectroscopy (SEM/EDS), and atomic force microscopy (AFM), revealing a dense, uniform microstructure with reduced surface roughness (63.99 nm) and increased particle density (30.2×10^6 particles/mm²) compared to the uncoated steel bar. Electrochemical measurements demonstrated a substantial decrease in corrosion current density (I_{corr}) for the coated specimens (1.11×10^{-7} A/cm²), along with the highest protection efficiency (92.29%). Electrochemical impedance spectroscopy (EIS) further confirmed the enhanced performance of the coated bars, with a superior total impedance resistance of 30,192 Ω·cm² and Warburg resistance of 18,320 Ω·cm² compared to uncoated ones (17,561 Ω·cm² and 9,363 Ω·cm²), respectively. These results highlight the potential of copper coatings as a viable solution for extending the service life of reinforced concrete structures in aggressive environments.

https://doi.org/10.53293/jasn.2025.7598.1341, Department of Applied Sciences, University of Technology - Iraq.

1. Introduction

Concrete is the most widely used construction material, providing inherent protection to reinforcing steel due to its highly alkaline environment. This alkalinity induces passivation of the steel, preventing the penetration of corrosive species (O_2, CO_2, Cl^-, and H_2O) in low water-to-cement ratio concrete. However, despite these protective factors, steel reinforcement remains susceptible to corrosion in environments characterized by high temperatures, high humidity, persistent moisture, and the presence of hygroscopic species such as airborne dust and salt particles, which accelerate deterioration. Therefore, it is crucial to maintain reinforced steel in a passive

and protective state, it is essential to use high-quality concrete and reduce contributing factors, including porosity, quality of mixing water and aggregate, permeability, freeze-thaw cycles, and sulfate content [1].

Many well-established methods exist for preventing corrosion risk, including the use of corrosion-resistant alloys, cathodic and anodic protection, inhibitors, and coatings. However, not all these methods are suitable for reinforced steel bars, because each method has its limitations. Corrosion-resistant steels are expensive and may not offer economical solutions for large-scale construction projects. Cathodic protection systems require continuous monitoring and electrical supply, making them complex and challenging to apply in standard construction structures. While corrosion inhibitors can delay the corrosion process, they may negatively interact with the surrounding concrete or gradually leach out, reducing their long-term effectiveness. Among the available methods, coatings stand out as the most practical and widely applicable solution, especially when applied during the steel manufacturing process. They provide an effective barrier against corrosion; however, conventional coatings are often susceptible to mechanical damage and degradation over time, particularly in harsh marine environments. As a result, choosing the most appropriate coating technique for protecting reinforced-steel bars remains a challenge [2-5]. Usually, the corrosion process of reinforcing steel begins when aggressive ions, especially chlorides, penetrate the concrete and reach the steel surface, initiating electrochemical reactions. The process starts with iron oxidation at anodic sites shown in **Eq. (1)** [6]:

$$\mathbf{Fe \rightarrow Fe^{2+} + 2e} \quad \textbf{(1)}$$

Simultaneously, oxygen from the environment is reduced at cathodic sites in the presence of moisture as shown in **Eq. (2)**:

$$\mathbf{1/2\ O_2 + 2e^- + H_2O \rightarrow 2OH^-} \quad \textbf{(2)}$$

These reactions create an alkaline environment that supports the formation of a passive ferric oxide-hydroxide layer as shown in **Eq. (3)**:

$$\mathbf{4Fe\ (OH)_2 + O_2 \rightarrow 2Fe_2O_3 \cdot H_2O + 2H_2O} \quad \textbf{(3)}$$

However, adsorbing the chloride ions on the protective layer leads to forming a soluble intermediate iron complex at the anodic sites as shown in **Eq. (4)**:

$$\mathbf{Fe^{2+} + 4Cl^- \rightarrow (FeCl_4)^{2-} + 2e} \quad \textbf{(4)}$$

After that, the former complex reacts with moisture to form ferrous hydroxide, with acid, leading to a reduced pH, adjusting the steel bar as shown in **Eq. (5)**:

$$\mathbf{(FeCl_4)^{2-} + 2H_2O \rightarrow Fe\ (OH)_2 + 2H^+ + 4Cl^-} \quad \textbf{(5)}$$

This process will be self-generated and does not require additional chloride ions. Additionally, the repeated cycle involving the reaction of iron ions with chloride ions continues until the protective layer is destroyed. As a result, pitting of the reinforcing steel occurs, representing an autocatalytic process that persists until a hole form in the reinforcing concrete. This is evident from the polarization resistance (R_P), which is calculated using the **Eq. (6)** [7, 8]:

$$\mathbf{R_p} = \frac{\mathbf{b_c \times b_a}}{\mathbf{2.303 \times i_{corr}\,(b_c + b_a)}} \quad \textbf{(6)}$$

The extent of corrosion can be quantified by the corrosion current density, and the effectiveness of any protective measure can be evaluated using protection efficiency (PE%) as shown in **Eq. (7)** [9, 10]:

$$\mathbf{PE}\ (\%) = \left[\mathbf{1} - \frac{\mathbf{i_{coated\ steel}}}{\mathbf{i_{uncoated\ steel}}}\right] \times \mathbf{100} \quad \textbf{(7)}$$

Moreover, the porosity percentage (PP% %) can be measured by **Eq. (8)** [11]:

$$\mathbf{PP\%} = \frac{\mathbf{R_{p,uncoated\ steel}}}{\mathbf{R_{p,coated\ steel}}}\ \mathbf{10}^{\frac{-\Delta \mathbf{E_{corr}}}{\mathbf{b_a}}} \times \mathbf{100} \quad \textbf{(8)}$$

In the production of steel rebar, hot rolling involves heating steel billets to a very high temperature and then passing them through a series of opposing rollers. The rollers are spaced closer together than the original thickness of the metal, which forces the billets to move forward while reducing their thickness and extending their length, all while maintaining their overall volume.

Numerous studies have investigated methods for protecting reinforced carbon steel bars embedded in concrete with different coating methods. In 2014, Criado *et al*. deposited polysiloxane hybrid films on steel bars by the dip coating method and compared the results with those obtained using the gel method. They evaluated the anticorrosion performance of these coatings in an alkaline medium (Simulated concrete pore solution) containing 3 wt.% sodium chlorides [12]. In 2016, Cedrim *et al*. coated reinforcing steel bar with Zinc and Zinc – nickel by electroplating method and they tested the corrosion performance in sodium chloride medium [13], While, Gunaselvi and Pazhani modified the reinforced carbon steel's surface by electroless method with nickel and tested the corrosion that accelerated with impressed voltage (12 V) [14]. In 2017, Pei *et al*. studied the corrosion performance of uncoated and coated reinforced steel embedded in mortar and immersed in 3.5% NaCl solution for one year using a new cementitious capillary crystalline waterproofing coating material that has self-healing properties through filling the small cracks and the void spaces [15]. In 2018, Mohamed *et al*. applied organic coatings with novel types of pigments to protect reinforced steel using a thin layer of ferrite to enhance the corrosion resistance by various electrochemical methods and the best protection was obtained with presence of ZnFe in coating [16], in 2019, Sohail *et al*. applied epoxy coating on reinforced steel for two years immersion in the simulated harsh chloride environment and tested the corrosion [17], Mukhopadhyay and Sahoo deposited (Ni) coating by electroless process incorporated with other metals to get Ni–P, Ni–P–W and Ni–P–Cu coatings and test corrosion in 3.5% NaCl solution [18], Fedosov *et al*. applied phosphate ($PO_4^{\equiv}$Coatings to protect reinforced steel in chloride solution with different degrees of aggressiveness [19], in 2020, Afshar *et al*. added pozzolanic materials such as fly ash, polypropylene fibers, silica fume, and industrial 2-dimethylaminoethanol as corrosion inhibitors to the concrete mixture to reduce the corrosion of reinforced steel. Their results showed that the combination of a zinc-rich epoxy primer with 25% fly ash, 10% silica fume, and 3% 2-dimethylaminoethanol inhibitors exhibited the highest corrosion resistance for the steel bars. In contrast, the Alkyd primer coating demonstrated the weakest performance [20]. Kamde and Pillai applied Cement-Polymer-Composite coating on reinforced steel under different conditions, including chloride concentrations, chloride thresholds and diffusion coefficients for the 6-year-old bridge. Their findings highlighted the importance of pre-preparation of the surface and cautioned against using the experimental coating without thorough pre-treatment, such as cleaning with sandblasting, to ensure effective adhesion and performance [21]. In 2021, Topçu *et al*. applied zinc and boron coatings using thermionic vacuum arc technique on reinforced steel in the concrete mixture in the mold [22]. Al-Negheimish *et al.* coated reinforced steel by alloying Zn with Al using hot dip galvanizing technique to test corrosion in chloride-contaminated concrete. The different concentrations of Al (10%, 15%, 20%, and 30%) investigated in the zinc alloy. The results showed that the 10% Al-90% Zn alloy (10AZ) provided the most effective corrosion protection [23]. Al-Dulaijan applied epoxy coating on reinforced steel embedded in concrete which exposed to chloride medium using different types of bars [24], Rooby *et al*. suggested a novel nanophase modified fly ash-based cement polymer coating for reinforced with different percentages of compositions including nano-$CaCO_3$, nano-SiO_2 and nano-ZrO_2. The long-term corrosion performance was evaluated using an impressed voltage test in a chloride-rich environment [25]. Ress *et al*. protected reinforced steel by modified epoxy coating with colophony microcapsules as corrosion inhibitors. The corrosion resistance was evaluated in both simulated concrete pore solution and 3.5 wt.% NaCl solution [26]. In 2022, Van Leeuwen *et al.* studied the effectiveness of continuous galvanizing for reinforced steel to improve product consistency, lower costs and increase throughput. The zinc coating provides abrasion resistance and durability, while also acting as a sacrificial layer to protect the underlying layer [27], Uzunömeroğlu *et al*. investigated the effectiveness of nanocoating to protect reinforced steel compared with conventional methods such as cathodic protection, epoxy coatings, and organic & inorganic inhibitors, the nanocoating comprising Zinc, Zinc-Boron and Zinc-Boron-

Nitrogen nanocrystals were applied using thermionic vacuum arc technique [28]. In 2023, El-Gawad *et al.* used modified feldspars as anticorrosive pigments that were prepared by chemical deposition with different oxides, including zinc oxide and vanadium oxide. This modification significantly enhanced the anticorrosive property of reinforced steel [29]. Matziaris *et al*. suggested a hybrid-based coating for reinforced steel in concrete, applied using a welding technique at approximately 400 °C. This approach enhances adhesion and durability while promoting sustainability through using both water-based and organic solvent-based polymeric matrices [30]. Das *et al*. applied alkali-activated slag coatings to protect reinforced steel in chloride-induced corrosion [31]. In 2024, Pokorný *et al*. applied plasma-sprayed Al_2O_3 coating on reinforced steel, followed by a top layer consisting of a Zr-based conversion coating and an organofunctional silane layer using 3-glycidyloxypropyltrimethoxysilane to enhance protection [32]. Marek *et al*. applied Zn-5Al coatings to reinforced steel using the hot dip technique at a high temperature [33], and Ghazaee *et al*. used glutamic acid as corrosion inhibitor to protect reinforced steel in a concrete pore solution contaminated chloride ion [34]. The present study aims to develop an efficient corrosion protection technique that can be easily incorporated into the steel bar manufacturing process. It involves copper (Cu) coating during hot rolling, creating a diffusion layer without affecting the steel's mechanical performance.

2. Experimental Procedure

2.1 The Materials

A steel bar according to ISO-6935-2:2015 standard was used with a diameter of 1.2 cm and a length of 13 cm. The steel's chemical composition by weight included 0.22 C, 0.6 Si, 1.6 Mn, 0.05 P, 0.05 S, 0.1 Cr, 0.1 Ni, 0.33 Cu, 0.01 Al, with the Balance being Fe. For Cu coating, copper powder obtained from "the Central Drug House (P) Ltd. Company" was used with a particle size ranging from 20 – 50 μm and purity of 99.6%. In this study, samples preparation involved using sulphate-resisting Portland cement (SRPC) with a chemical composition of (63.6% CaO, 19.35% SiO_2, 3.98% Al_2O_3, 5.03% Fe_2O_3, 1.71% SO_3, 3.32% MgO, 0.02% Cl, 1.1% I.R, 3.05% L.O.I, 72.99% C_3S, 0.4% C_2S, 2.05% C_3A, and 15.31% C_4AF). Additionally, black-crushed gravel with a maximum size of 10 mm was used as the coarse aggregate, while sand containing 0.4% SO_3 served as the fine aggregate. The quantities of concrete mixture to prepare these specimens are listed in **Table 1**.

Table 1. The quantities of the concrete mixture.

Cement (Kg/m^3)	Sand (Kg/m^3)	Gravel (Kg/m^3)	Water (L/m^3)
310	720	1190	154.5

The reinforcing steel bars were positioned vertically in cubic molds measuring 10×10×10 cm^3, as seen in **Fig. 1**.

Figure 1. Cubic concrete specimens before and after casting.

During the casting process, an electrical vibrator table was used to eliminate air bubbles and ensure proper compaction. All Concrete samples were unmolded 48 hours after casting and subsequently cured in tap water for 28 days. After that, all the reinforced concrete specimens were partially immersed in seawater 3.5 wt.% NaCl with a pH value of about 6.8 up to 5 mm below the top surface. The exposure lasted for 28, 56, and 90 days to evaluate the corrosion resistance before and after applying the coating.

2.2 Coating Process

The coating technique in this study was performed during the hot rolling process, where carbon steel bars were heated to a temperature range of 1000 and 1050°C. Copper powder was then pumped at a pressure of 116 bar through two nozzles positioned above and below the reinforcing bar, depositing the powder onto the rebar's surface. Upon contact with the heated steel, the copper powder melted and formed a uniform protective coating layer across the entire surface of the rebar.

2.3 Measurements

To characterize the coated surface, XRD, SEM/EDS, and AFM were utilized. The structural state of the coating was investigated using X-ray diffraction (XRD) from Shimadzu, Japan, at a scanning rate of $1^\circ\ \mathrm{min}^{-1}$ Within an angular range of 10°–90°. Scanning electron microscopy (SEM) paired with energy-dispersive spectroscopy (EDS) from Thermo Fisher Scientific Company, USA, was used to analyze the surface morphology and the elemental compositions. Additionally, an atomic force microscope (Flexafm-Axiom) from Nanosurf AG, Switzerland, provided high-resolution images to evaluate surface topography and roughness.

3. Corrosion Measurements

Electrochemical measurements were carried out using a Potentiostat from Corrtest company (model: CS350M) employing a three-cell set-up. The system consists of a reference electrode Calomel (Ag/AgCl), A counter electrode Platinum (Pt), and a working electrode (carbon steel samples) as illustrated in **Fig. 2**, Tafel plots were recorded for each sample, and the data was measured by applying Tafel extrapolation method to determine key corrosion parameters, including the corrosion potential (E_{corr}), corrosion current density (i_{corr}), and Tafel slope for both the cathodic (b_c) and anodic (b_a) section. Then, protection efficiency, polarization resistance, and porosity percentage were calculated [35, 36]. Electrochemical impedance spectroscopy (EIS) was also estimated by recording Nyquist plots for coated and uncoated steel samples to measure the different resistances for solution, charge transfer and diffusion.

Figure 2. Electrochemical measurements using a three-electrode cell.

4. Results and Discussion

4.1 Characterization of Coated Surface

XRD analysis was used to obtain the results illustrated in **Fig. 3a and b**. In **Fig. 3a**, the distinct peaks corresponding to steel are observed at 2θ values of 43.76°, 59.84°, 64.28° and 81.68°. This peak aligns with reference data from JCPDS card No. 35-1357, while in **Fig. 3b**, the main peaks of Cu are noticed at 2θ values of 43.16°, 50.36° and 74.28° corresponding to JCPDS card No. 04-0836. Other peaks shown in the diffraction pattern are attributed to the formation of the ($CuFe_2O_4$) phase, which appears at 36.28°, 61.36° and 90.604° as identified by JCPDS card No. 25-0283. This phase was created during the coating process, where elevated temperature promotes diffusion within the steel's surface layer, enhanced by oxygen, as shown by T. Ramaprasad *et al*., who prepared ($CuFe_2O_4$) nanoparticles through a low-temperature hydrothermal method [37].

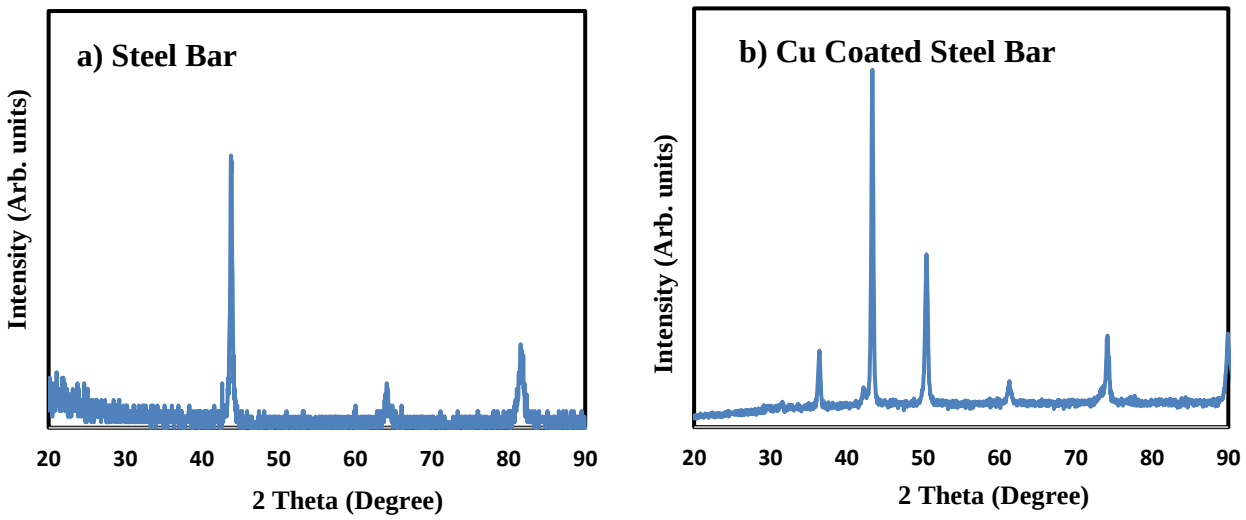

Figure 3. XRD pattern for steel bar (**a**) and Cu coated steel (**b**).

SEM was used to analyze the surface morphology of uncoated and Cu-coated steel samples. The SEM images of the uncoated steel are shown in **Fig. 4a**, revealing irregular edges associated with the structural features of steel bars used in construction to enhance adhesion with cement paste, resulting in a rough surface. In contrast, **Fig. 4b** presents the SEM images of the Cu-coated steel, showing a homogeneous, dense layer similar in size to the SEM images of spinel oxides (CuO. $CuFe_2O_4$). This is in agreement with Linh *et al*. when they developed this core–shell structure as a photoelectrode [38].

EDS in **Fig. 5a**, revealed the elemental composition of the uncoated steel rebar, confirming the presence of all base elements, with iron (86.7 wt.%) and carbon (10.8 wt.%) as the primary constituents, while in **Fig. 5b**, the EDS analysis of the coated sample, where copper exhibited the highest weight percentage (48.3%) due to its presence in the form of Cu, CuO, and $CuFe_2O_4$ followed by carbon (47.2%), which appears as a distinct element located at the grain boundaries.

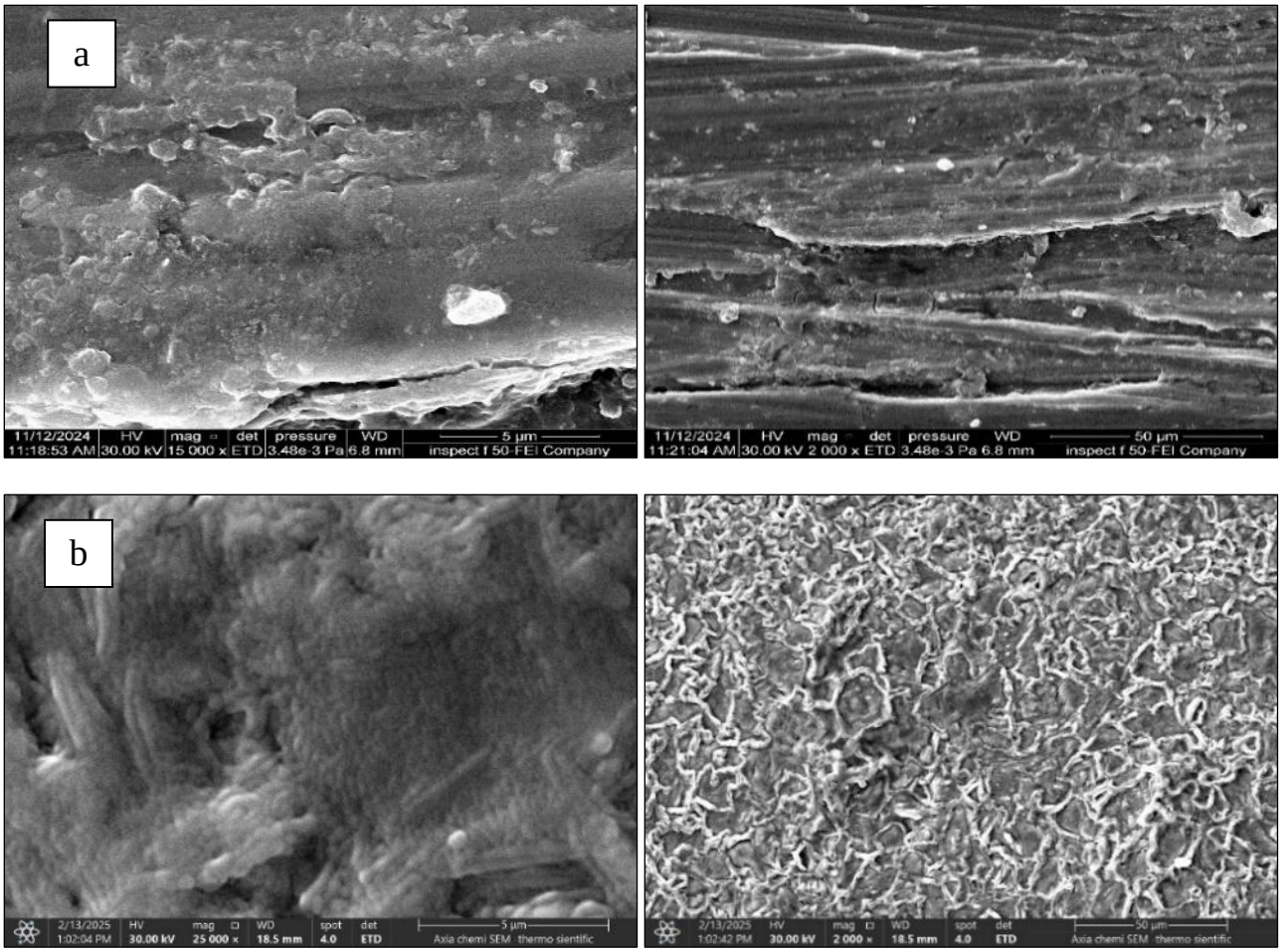

Figure 4. SEM images of (**a**) uncoated steel and (**b**) copper-coated steel.

Atomic force microscopy (AFM) was employed to analyze the topography of both coated and uncoated steel bar samples, as shown in **Fig. 6 and Fig. 7**. The AFM images of the steel bar, presented in both two and three-dimensional views, highlight the valley-like surface features characteristic of reinforced steel bars. These surface features are essential for ensuring proper adhesion with cement paste, resulting in a high surface roughness of 133.6 nm. On the other hand, the AFM scan of the Cu-coated steel bar revealed a distinctive Cauliflower-like structure in both 2D and 3D imaging. This structure is attributed to the formation of a Cu layer doped with Fe from the substrate and O from the oxidation process. These findings are consistent with the observations of Anant *et al*., who reported a similar hill-and-valley structure in AFM images of $CuFe_2O_4$. Thin films, characterized by agglomerated grains and dense film formation [39]. The Cu-coated steel surface exhibited a reduced roughness of 63.99 nm. This decrease in roughness offers a significant advantage in reducing corrosion by minimizing anodic and cathodic sites.

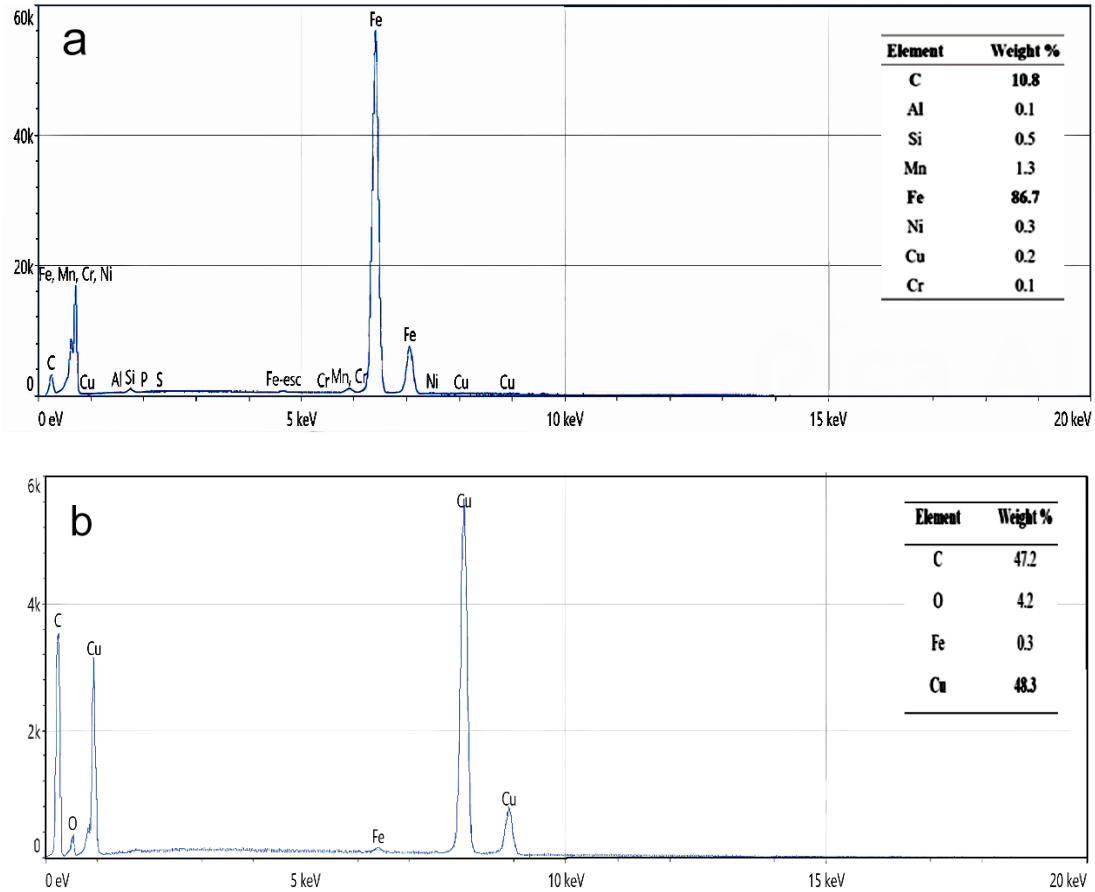

Figure 5. EDS analysis of (a) uncoated steel and (b) Cu-coated steel.

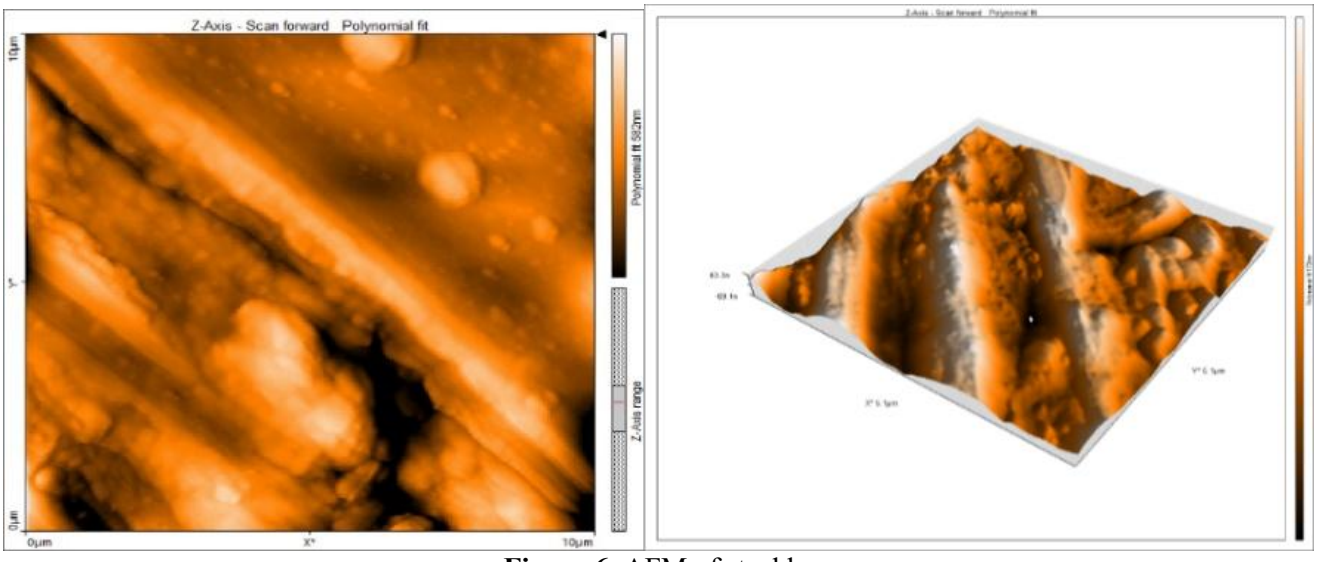

Figure 6. AFM of steel bar.

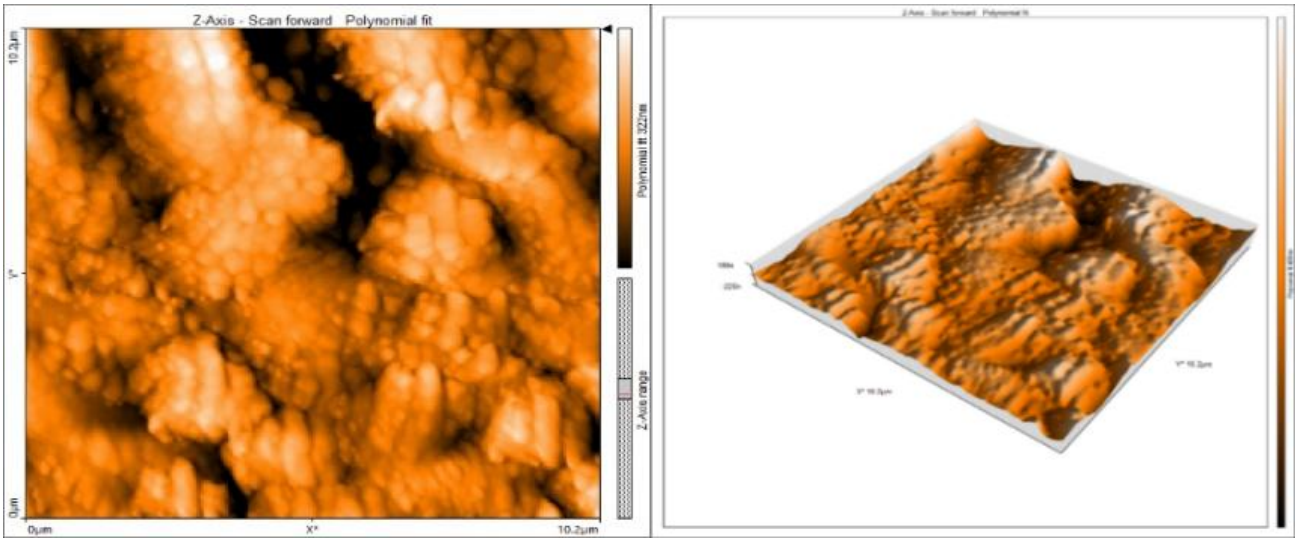

Figure 7. AFM of Cu coated steel bar.

The chart of particle distribution for the steel bar and the coated sample, shown in **Fig. 8a and b**, indicates that the uncoated steel bar exhibited the largest particle distribution area, with a mean particle diameter of 195.7 nm. In contrast, the Cu-coated steel shows a dominant area corresponding to a smaller percentage of particles, resulting in a reduced mean diameter of 51.17 nm. This decrease in particle size after the coating process confirms effective surface coverage by copper atoms, along with the formation of the $CuFe_2O_4$ phase, which collectively contributes to a reduced risk of corrosion.

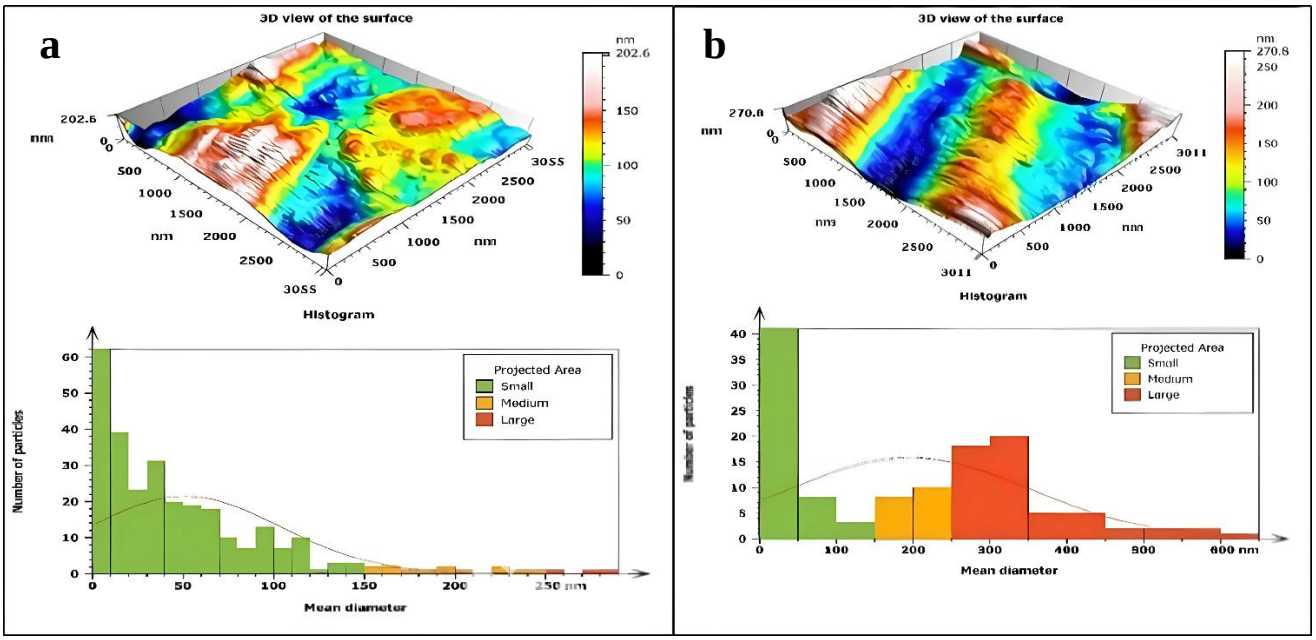

Figure 8. Particle distribution chart of steel bar (a) and Cu coated steel (b).

According to the AFM scan data, the number of particles recorded was 125 for the uncoated steel surface and 282 for the coated surface, with particle densities of 13,786,312 particles/mm² and 30,211,328 particles/mm², respectively. This increase in particles, along with density, suggests the formation of a more compact and uniform surface layer following the coating process. Other data provided by the AFM analysis are listed in **Table 2**.

Table 2. Height parameters of coated and uncoated steel rebar samples.

Parameter-steel	Steel bar	Cu-coated bar
Root-mean-square height (Sq)	169.4 nm	83.33 nm
Maximum peak height (Sp)	607.1 nm	242.6 nm
Maximum pit depth (Sv)	608.1 nm	351.6 nm
Maximum height (Sz)	1215 nm	594.1 nm
Arithmetic mean height (Sa)	133.6 nm	63.99 nm

The average Vickers microhardness of the uncoated steel rebar surface was 195.8 HV, while that of the copper-coated surface exhibited a lower hardness value of 57.8 HV. However, the high-temperature conditions during the coating process facilitated the diffusion and interaction of copper with other elements of the steel substrate, such as iron and oxygen, forming a low-porosity coating layer. Although copper is inherently softer, the reduced porosity of the coating contributed to an improvement in its hardness relative to pure copper, as hardness generally increases when porosity decreases [40].

4.2 Corrosion Behavior

The main objective of this work is to reduce the corrosion risk estimated by recorded polarization curves. **Fig. 9, Fig. 10, and Fig. 11** show the Tafel plots for uncoated and coated steel bars after three different immersion periods (28, 56 and 90 days). Generally, the corrosion potential of steel bars varies with immersion time, while the corrosion current increases with increasing time of immersion due to prolonged exposure to aggressive species. These species pass through the cement paste and reach the steel surface, leading to the destruction of the passive film. The polarization resistance (R_p) of the Cu-coating was measured using **Eq. (6)**.

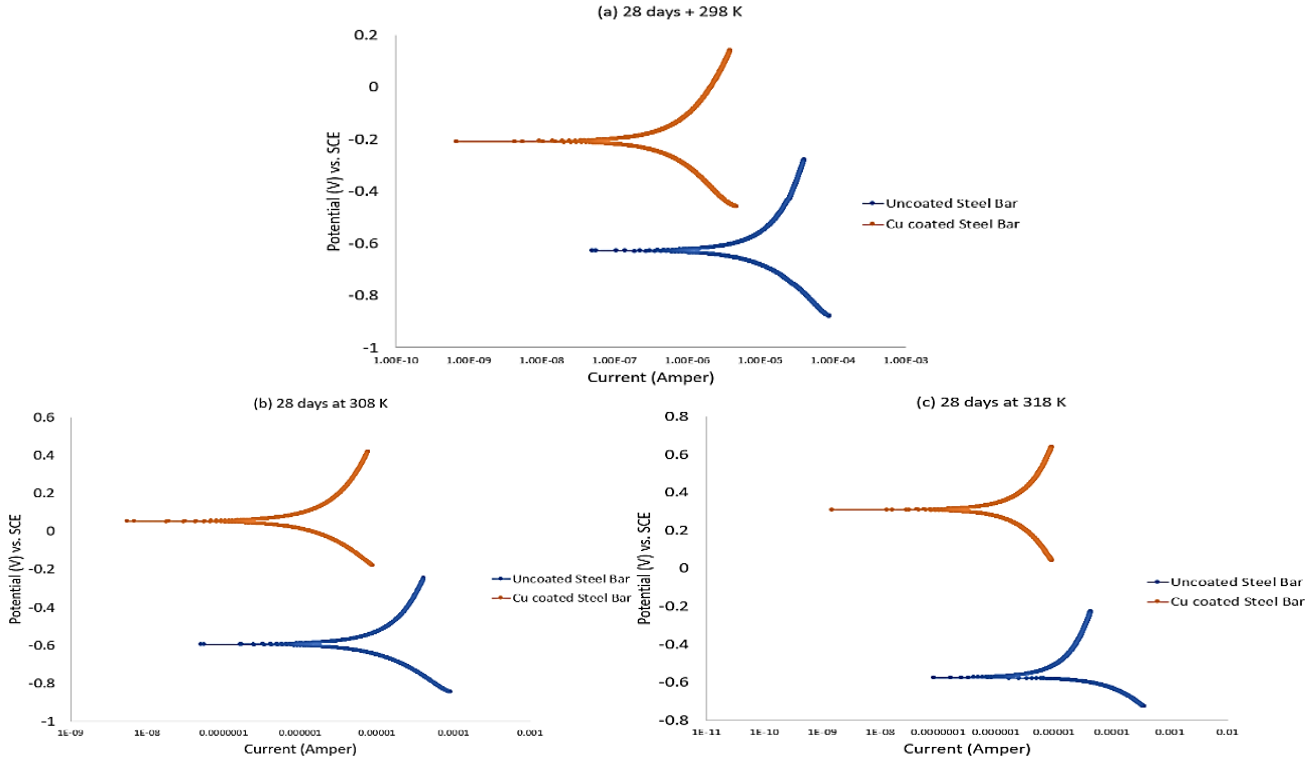

Figure 9. Tafel plots for a 28-day immersion at three different temperatures.

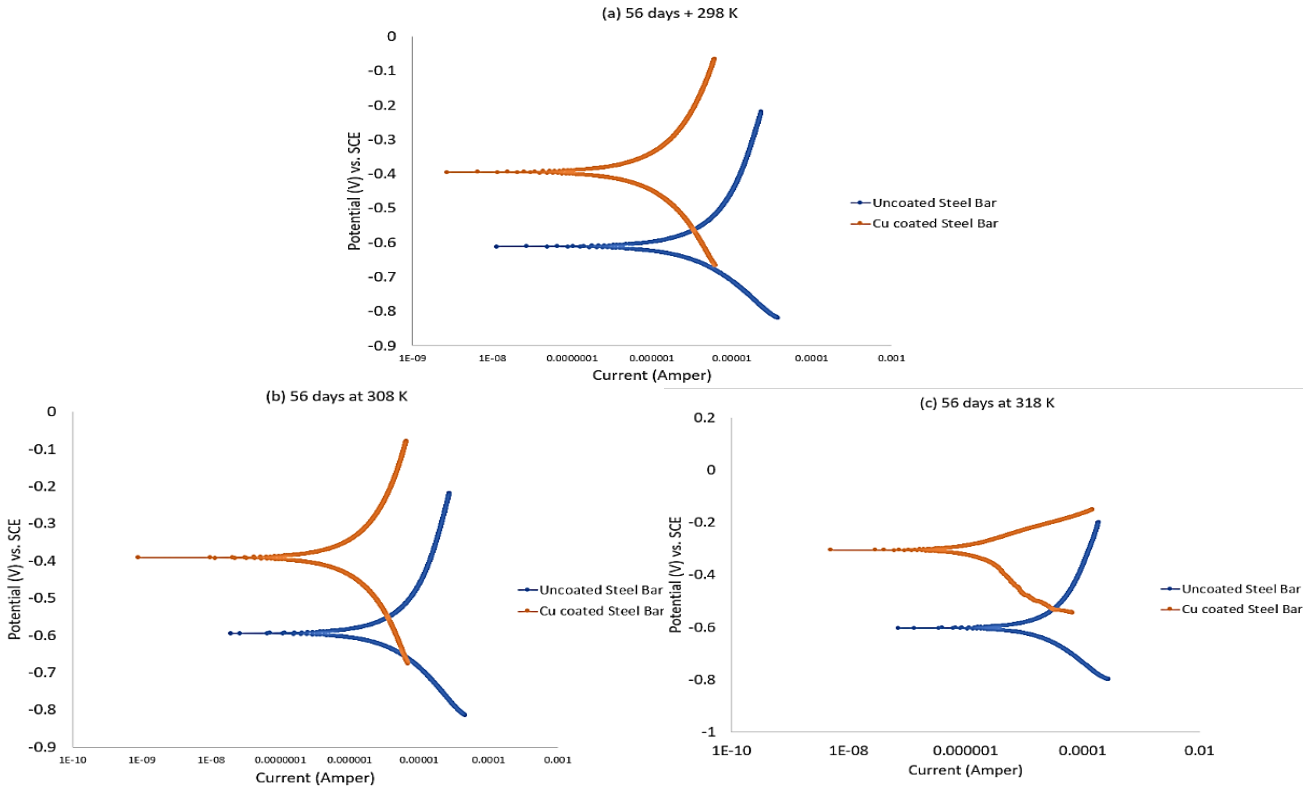

Figure 10. Tafel plots for an immersion duration of 56 days at three temperatures.

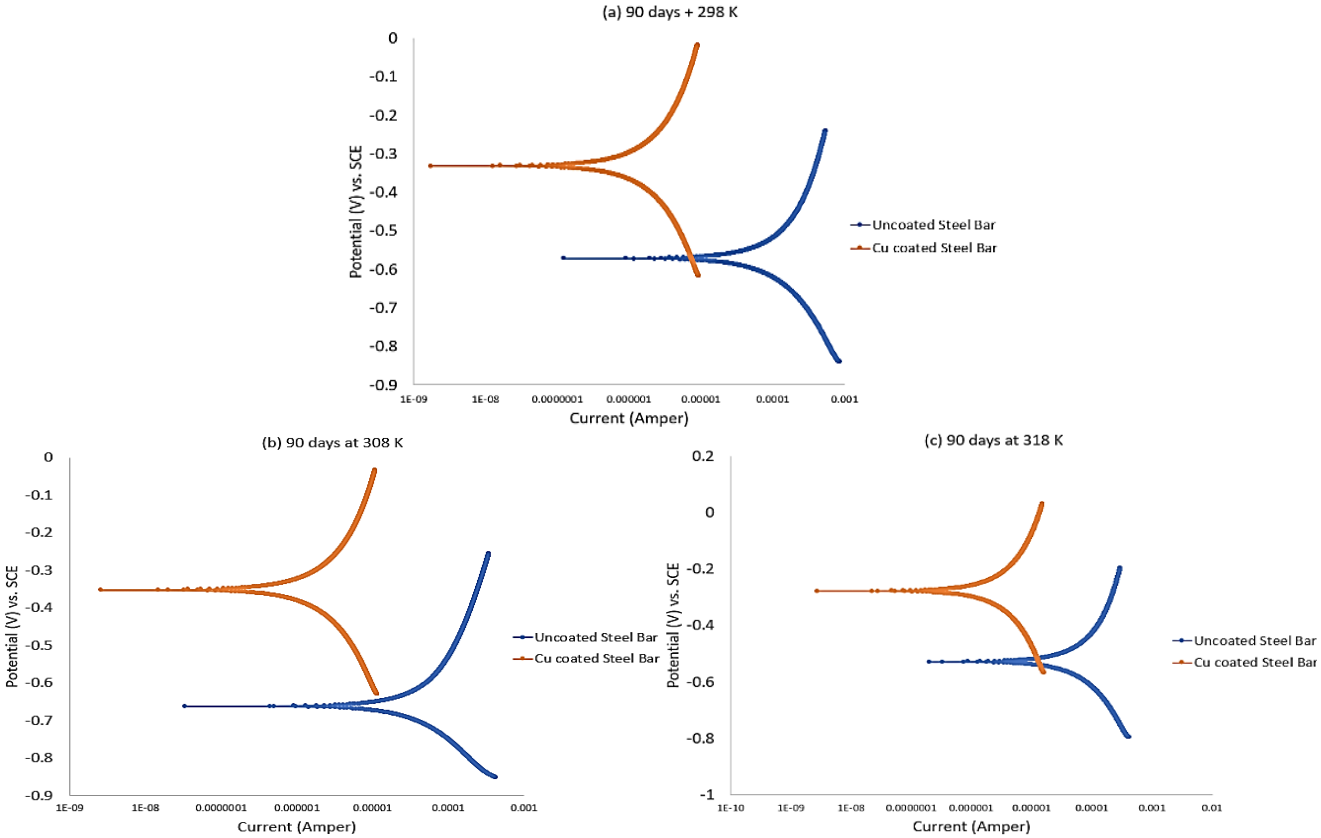

Figure 11. Tafel plots for a 90-day immersion time at three varying temperatures.

Applying a diffused copper coating on reinforced steel bars provided some protection, thereby extending the lifetime of the bars. Polarization measurement confirmed this enhancement as shown by the polarization curves and the data presented in **Table 3, Table 4, and Table 5**. The results showed a shift in the corrosion potential toward more noble values and a noticeable reduction in corrosion current density. These changes indicate increased corrosion resistance and improved protection efficiencies (PE%), which were calculated by **Eq. (7)**.

Table 3. Corrosion data for both uncoated and coated steel rebar after an immersion time of 28 days at different temperatures.

Coating type	Temp. (K)	$-E_{corr}$ (V)	$i_{corr}x10^{-7}$ ($A.cm^{-2}$)	$-b_c$ ($mV.dec^{-1}$)	$+b_a$ ($mV.dec^{-1}$)	IE (%)	$R_p\times 10^{+4}$ ($\Omega.cm^2$)
	298	0.628	14.4	40.72	39.86	-	0.608
Uncoated	308	0.595	16.26	41.71	21.40	-	0.378
	318	0.576	18.41	37.92	25.58	-	0.360
	298	0.208	1.11	54.50	49.08	92.29	10.116
Cu	308	-0.053	4.32	37.99	37.14	73.45	1.891
	318	0.309	5.28	42.56	42.14	71.29	1.741

Table 4. Corrosion data for uncoated and coated steel bars after a 56-day immersion period at varying temperatures.

Coating type	Temp. (K)	$-E_{corr}$ (V)	$i_{corr}x10^{-7}$ ($A.cm^{-2}$)	$-b_c$ ($mV.dec^{-1}$)	$+b_a$ ($mV.dec^{-1}$)	IE (%)	$R_p\times 10^{+4}$ ($\Omega.cm^2$)
	298	0.612	15.154	297.92	727.42	-	0.606
Uncoated	308	0.595	16.682	31.04	38.39	-	0.447
	318	0.604	17.5263	31.62	36.34	-	0.419
	298	0.395	3.447	38.63	34.50	77.25	2.299
Cu	308	0.392	4.368	34.42	28.55	73.81	1.553
	318	0.305	5.119	35.84	34.15	70.79	1.485

Table 5. Corrosion data for uncoated and coated steel bars after 90 days of immersion at different temperatures.

Coating type	Temp. (K)	$-E_{corr}$ (V)	$i_{corr}x10^{-7}$ ($A.cm^{-2}$)	$-b_c$ ($mV.dec^{-1}$)	$+b_a$ ($mV.dec^{-1}$)	IE (%)	$R_p\times 10^{+4}$ ($\Omega.cm^2$)
	298	0.572	17.8285	36.61	49.27	-	0.512
Uncoated	308	0.664	18.716	276.93	604.79	-	0.441
	318	0.529	19.2937	52.41	59.68	-	0.628
	298	0.332	9.324	35.51	39.15	47.70	0.868
Cu	308	0.353	10.326	28.29	32.35	44.82	0.635
	318	0.278	11.225	32.06	30.84	41.82	0.608

The PE% data indicate that the copper coating exhibited the highest corrosion protection efficiency at the lowest temperature (298 K), with efficiency declining as the temperature increased. This trend suggests that the protective effect of copper coating is more effective under cooler conditions. The presence of copper on the steel surface promoted the formation of copper oxides during exposure to the electrolyte (Seawater). In the oxygen-rich environment, two main corrosion products were formed, including cuprous oxide (Cu_2O) and cupric oxide (CuO), both contributing to the protective barrier that slows down further corrosion. The scale of these two compounds depended on their thermodynamic stability, which was determined by a series of reactions **Eq. (9), Eq. (10), Eq. (11), Eq. (12), and Eq. (13)** [41]:

$$\mathbf{2Cu + 2OH^- \rightarrow Cu_2O + H_2O + 2e} \quad \mathbf{(9)}$$

$$\mathbf{Cu_2O + 2OH^- \rightarrow 2CuO + H_2O + 2e} \quad \mathbf{(10)}$$

$$Cu + 2OH^- \rightarrow CuO + H_2O + 2e \quad (11)$$

$$Cu_2O + H_2O + 2e \rightarrow 2Cu + 2OH^- \quad (12)$$

$$2CuO + H_2O + 2e \rightarrow Cu_2O + 2OH^- \quad (13)$$

These reactions can create brittle scale, which influences the protection of the steel surface. The data in **Table 6** show the values of the porosity percentage (PP%) estimated by **Eq. (8)** and confirm the decrease in the protectiveness of copper-oxide with increasing temperature and immersion period.

Table 6. The porosity percentages for coating with copper at different immersion periods.

Temp. (K)	PP%		
	28 days	56 days	90 days
298	5.866	26.341	59.651
308	18.643	28.434	69.562
318	20.186	27.685	104.294

The second measurement of electrochemical behavior can be estimated by EIS, which represents one of the most important electrochemical measurements. In this method, impedance in a circuit is measured in resistance units to assess mass-transfer, charge-transfer, and diffusion processes, in addition to evaluating the material properties that may influence the conductance, capacitance or resistance of an electrochemical system. In the current study, EIS measurements were performed for groups immersed for 28 and 56 days at 298 K. **Fig. 12** illustrates the EIS data as a Nyquist plot for uncoated and Cu coated steel bars immersed for 28 days at 298 K, showing the characteristic semicircle shape. The plot reveals the presence of three resistances: solution resistance (R_s), double-layer capacitance at the electrode surface (C_{dl}), charge-transfer resistance (R_{ct}), and Warburg resistance (Z_w). An increase in the semicircle's diameter corresponds to an increase in charge-transfer resistance (R_{ct}), indicating that the Cu coated steel exhibited the largest diameter compared to the uncoated sample. This trend is represented in **Table 7**, which shows higher solution resistance and charge transfer for coated steel, in agreement with the results of the Tafel polarization test. A similar behavior was observed after 56 days of immersion at 298 K (**Fig. 13**), with higher resistance for the coated specimen compared to the uncoated one, as listed in **Table 8**. Additionally, the resistance at 28 days was higher than that at 56 days, indicating greater diffusion at the later time point.

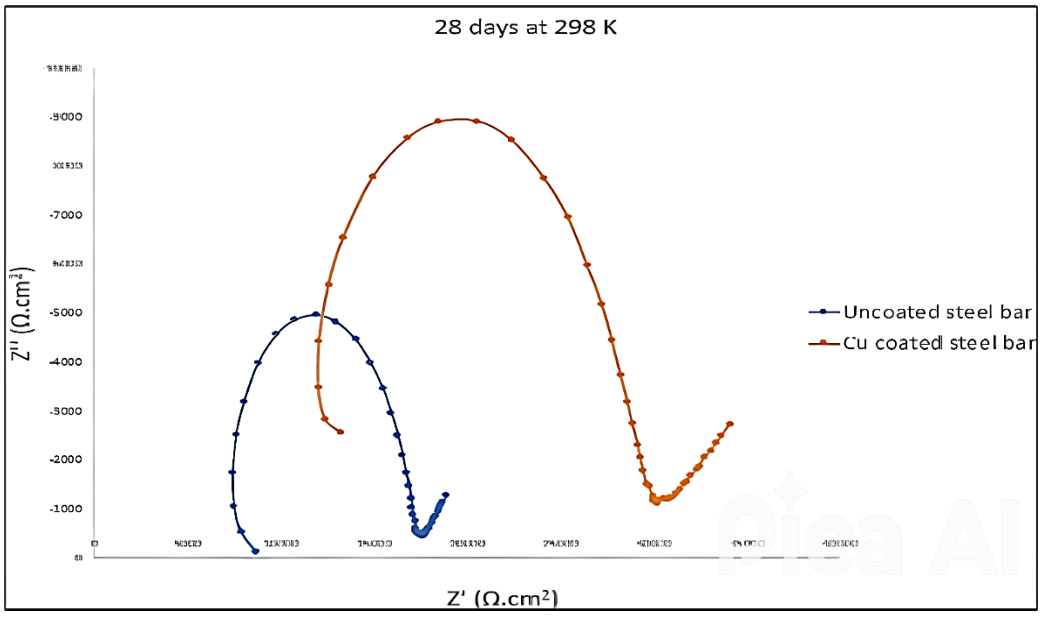

Figure 12. Nyquist plots for samples immersed for 28 days at 298 K.

Table 7. The data of EIS for specimens immersed for 28 days at 298 K.

Specimen	R_s ($\Omega.cm^2$)	$R_s + R_{ct}$ ($\Omega.cm^2$)	Z_w ($\Omega.cm^2$)
Uncoated bar	7520	17561	9363
Cu coated bar	12846	30192	18320

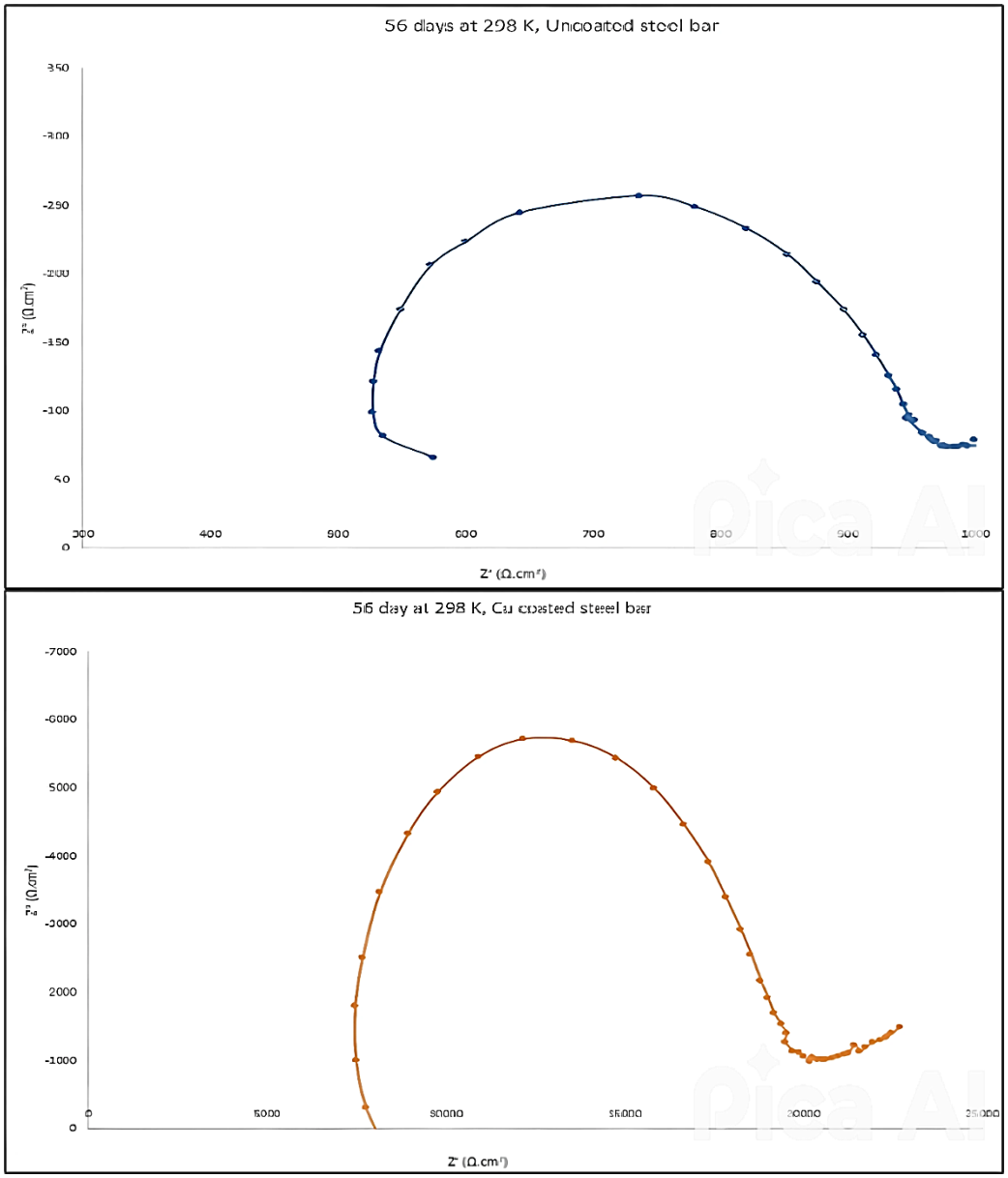

Fig. 13. Nyquist plots for a 56-day immersion period at 298 K.

Table 8. The data of EIS for specimens immersed for 56 days at 298 K.

Specimen	R_s ($\Omega.cm^2$)	$R_s + R_{ct}$ ($\Omega.cm^2$)	Z_w ($\Omega.cm^2$)
Uncoated bar	255.95	975.5	1106
Cu coated bar	8636	19873	25425

5. Conclusion

This study confirmed that thermally sprayed copper coatings significantly improve the corrosion resistance of reinforcing steel bars in chloride-rich environments. Surface characterization showed a notable reduction in roughness from 133.6 nm for uncoated steel to 63.99 nm for Cu-coated steel, along with an increase in particle density from 13.78×10^6 to 30.2×10^6 particles/mm², forming a dense protective layer. Electrochemical tests revealed significant improvements, particularly after 28 days of immersion at 298 K, where the Cu-coated specimens achieved the best performance with a corrosion current density of 1.11×10^{-7} A/cm², a polarization resistance of 10.12×10^4 Ω·cm², and a protection efficiency of 92.29 % EIS results under the same conditions confirmed enhanced charge-transfer resistance, with the coated samples exhibiting the highest total impedance of 30.192Ω·cm², and Warburg resistance of 18.320 Ω·cm². In addition, the average microhardness of the coating surface was 57.8 HV, highlighting the mechanical stability of the coating layer. The formation of $CuFe_2O_4$ contributed to the barrier effect, preventing chloride ion penetration and minimizing corrosion activity. Overall, these findings support the potential application of copper-coated reinforcement as a viable strategy for improving the durability of concrete structures in aggressive environments.

References

[1] Z. Li, X. Zhou, H. Ma, and D. Hou, *Advanced concrete technology*. John Wiley & Sons, 2022.

[2] A. A. Hashim, R. Anaee, and M. S. Nasr, "Enhancing the sustainability, mechanical and durability properties of recycled aggregate concrete using calcium-rich waste glass powder as a supplementary cementitious material: An experimental study and environmental assessment," *Sustain. Chem. Pharm.*, vol. 44, p. 101985, 2025.

[3] A. A. Hashim, R. Anaee, and M. S. Nasr, "Improving the Mechanical, Corrosion Resistance, Microstructural and Environmental Performance of Recycled Aggregate Concrete Using Ceramic Waste Powder as an Alternative to Cement," *Ceramics*, vol. 8, no. 1, p. 11, 2025.

[4] P. Jayaweera, D. M. Lowe, A. Sanjurjo, K. H. Lau, and L. Jiang, "Corrosion-resistant metallic coatings on low carbon steel," *Surf. coatings Technol.*, vol. 86, pp. 522–525, 1996.

[5] L. Zhang, J. Li, and H. Qiao, "Effect of copper tailing content on corrosion resistance of steel reinforcement in a Salt Lake environment," *Materials (Basel).*, vol. 12, no. 19, p. 3069, 2019.

[6] M. H. Hafiz, R. A. Majed, R. S. Noor, and M. A. Wehib, "Phenylenediamine as inhibitor in sour water at oil refinery," *Int. J. Electrochem. Sci.*, vol. 8, no. 12, pp. 12402–12416, 2013.

[7] A. M. H. Al-Ghaban, H. A. Abdullah, R. A. Anaee, S. A. Naser, and A. A. Khadom, "Expired butamirate drug as eco-friendly corrosion inhibitor for aluminum in seawater: Experimental and theoretical studies," *J. Eng. Res.*, vol. 12, no. 3, pp. 299–309, 2024.

[8] S. A. A. Maged, R. A. Anaee, and M. T. Mathew, "Negative effect of calcium tablets on the corrosion of a Co–Cr–Mo alloy as an implant," *Int. J. Corros. Scale Inhib.*, vol. 12, no. 1, pp. 275–291, 2023.

[9] H. A. Abdullah, R. A. Anaee, and A. A. Khadom, "Expired Metheprim drug as a corrosion inhibitor for aluminum in 1 M HCl solution: Experimental and theoretical studies," *Int. J. Corros. Scale Inhib*, vol. 11, no. 3, pp. 1355–1373, 2022.

[10] R. A. M. Anaee, "Thermodynamic and kinetic study for corrosion of Al-Si-Cu/Y_2O_3 composites," *Asian J. Chem.*, vol. 26, no. 14, pp. 4469–4474, 2014.

[11] R. A. Anaee, A. A. Abdulkarim, M. T. Mathew, and H. M. Jedy, "The effect of Nb_2O_5-Ni coatings on the microstructural and corrosion behavior on carbon steel for marine application," *J. Bio-and Tribo-Corrosion*, vol. 7, no. 1, p. 1, 2021.

[12] M. Criado, I. Sobrados, J. Sanz, and J. M. Bastidas, "Steel protection using sol–gel coatings in simulated concrete pore solution contaminated with chloride," *Surf. Coatings Technol.*, vol. 258, pp. 485–494, 2014.

[13] F. A. Cedrim, V. L. S. Almeida, C. A. C. Souza, M. D. Jesus, and D. V Ribeiro, "Effects of the zinc and zinc-nickel alloys electroplating on the corrodibility of reinforced concrete rebars," *Rev. IBRACON Estruturas e Mater.*, vol. 9, no. 04, pp. 595–605, 2016.

[14] S. Gunaselvi and K. C. Pazhani, "Corrosion control of steel rebars using electroless nickel coating," *Trans. Indian Inst. Met.*, vol. 69, pp. 859–868, 2016.

[15] X. Pei, M. Noel, M. Green, A. Fam, and G. Shier, "Cementitious coatings for improved corrosion

resistance of steel reinforcement," *Surf. Coatings Technol.*, vol. 315, pp. 188–195, 2017.
[16] M. G. Mohamed, N. M. Ahmed, and W. M. Abd El-Gawad, "Corrosion protection performance of reinforced steel coated with paints based on waste materials," *Anti-Corrosion Methods Mater.*, vol. 65, no. 4, pp. 368–374, 2018.
[17] M. G. Sohail, M. Salih, N. Al Nuaimi, and R. Kahraman, "Corrosion performance of mild steel and epoxy coated rebar in concrete under simulated harsh environment," *Int. J. Build. Pathol. Adapt.*, vol. 37, no. 5, pp. 657–678, 2019.
[18] A. Mukhopadhyay and S. Sahoo, "Corrosion protection of reinforcement steel rebars by the application of electroless nickel coatings," *Eng. Res. Express*, vol. 1, no. 1, p. 15021, 2019.
[19] S. Fedosov, V. Roumyantseva, and V. Konovalova, "Phosphate coatings as a way to protect steel reinforcement from corrosion," in *MATEC Web of Conferences*, EDP Sciences, 2019, p. 126.
[20] A. Afshar, S. Jahandari, H. Rasekh, M. Shariati, A. Afshar, and A. Shokrgozar, "Corrosion resistance evaluation of rebars with various primers and coatings in concrete modified with different additives," *Constr. Build. Mater.*, vol. 262, p. 120034, 2020.
[21] D. K. Kamde and R. G. Pillai, "Effect of surface preparation on corrosion of steel rebars coated with cement-polymer-composites (CPC) and embedded in concrete," *Constr. Build. Mater.*, vol. 237, p. 117616, 2020.
[22] İ. Topçu, A. Uzunömeroğlu, and S. Pat, "Enhancing the Corrosion Resistance of Reinforced Concrete Rebar by the Implementation of Anti-corrosive Coatings with Using TVA System," 2021.
[23] A. Al-Negheimish, R. R. Hussain, A. Alhozaimy, and D. D. N. Singh, "Corrosion performance of hot-dip galvanized zinc-aluminum coated steel rebars in comparison to the conventional pure zinc coated rebars in concrete environment," *Constr. Build. Mater.*, vol. 274, p. 121921, 2021.
[24] S. U. Al-Dulaijan, "Corrosion-resistance evaluation of coated and specialty bars," *Eur. J. Environ. Civ. Eng.*, vol. 26, no. 12, pp. 5821–5842, 2022.
[25] D. R. Rooby, T. N. Kumar, M. Harilal, S. Sofia, R. P. George, and J. Philip, "Enhanced corrosion protection of reinforcement steel with nanomaterial incorporated fly ash based cementitious coating," *Constr. Build. Mater.*, vol. 275, p. 122130, 2021.
[26] J. Ress, U. Martin, J. Bosch, and D. M. Bastidas, "Protection of carbon steel rebars by epoxy coating with smart environmentally friendly microcapsules," *Coatings*, vol. 11, no. 2, p. 113, 2021.
[27] M. C. van Leeuwen, D. Lai, G. Kong, and M. Gagné, "Continuous Galvanized Reinforcing Steel in Concrete Structures," in *IABSE Congress Report*, 2022, pp. 622–627.
[28] A. Uzunömeroğlu, A. R. Boğa, S. Pat, and İ. B. Topçu, "Improving the corrosion resistance of reinforcement embedded in concrete with high strength zinc, Zinc-Boron and Zinc-Boron-Nitrogen nanocrystal composite coating," *Arab. J. Sci. Eng.*, vol. 47, no. 10, pp. 12789–12802, 2022.
[29] W. M. A. El-Gawad, E. A. Mossalam, and M. Gharieb, "Enhancing corrosion resistance in reinforced concrete structures by using innovative eco-friendly composite pigments," *Innov. Infrastruct. Solut.*, vol. 8, no. 12, p. 320, 2023.
[30] K. Matziaris, E. Tsampali, E. Tsardaka, and M. Stefanidou, "Hybrid protective coatings for construction steel bars," *ce/papers*, vol. 6, no. 5, pp. 990–995, 2023.
[31] C. S. Das, H. Zheng, X.-L. Zhao, and J.-G. Dai, "Corrosion inhibition of steel reinforcements in seawater sea sand concrete by alkali-activated slag based coatings," *Constr. Build. Mater.*, vol. 394, p. 132210, 2023.
[32] P. Pokorný, N. Prodanovic, K. Hurtig, V. Steinerová, J. Fojt, M. Janata *et al.*, "Corrosion Properties and Bond Strength in Normal Strength Concrete of Al_2O_3 Plasma-Sprayed Plain Bars with ZrCC/Organofunctional Silane Coating," *Buildings*, vol. 14, no. 6, p. 1543, 2024.
[33] A. Marek, V. Steinerová, P. Pokorný, H. Kania, and F. Berger, "High-temperature Zn-5Al hot dip galvanizing of reinforcement steel," *Coatings*, vol. 14, no. 8, p. 959, 2024.
[34] A. Ghazaee, S. Pour-Ali, S. Mahdavi, R. Tavangar, and M. Khalili, "Corrosion inhibition of steel rebar in chloride-contaminated concrete pore solution: Ecofriendly glutamic acid inhibitor and its synergy with galvanized coating," *Inorg. Chem. Commun.*, vol. 167, p. 112832, 2024.
[35] H. A. Abdulaah, A. M. Al-Ghaban, R. A. Anaee, A. A. Khadom, and M. M. Kadhim, "Cerium-tricalcium phosphate coating for 316L stainless steel in simulated human fluid: Experimental, biological, theoretical, and electrochemical investigations," *J. Electrochem. Sci. Eng.*, vol. 13, no.

1, pp. 115–126, 2023.

[36] S. A. Naser, R. A. Anaee, and H. A. Jaber, "Gd–Ni–Ti coating to reduce corrosion of SS 316L for bioapplication," *Adv. Mater. Process. Technol.*, pp. 1–12, 2024.

[37] T. Ramaprasad, R. Jeevan Kumar, U. Naresh, M. Prakash, D. Kothandan, and K. Chandra Babu Naidu, "Effect of pH value on structural and magnetic properties of $CuFe_2O_4$ nanoparticles synthesized by low temperature hydrothermal technique," *Mater. Res. Express*, vol. 5, no. 9, p. 095025, Aug. 2018.

[38] L. Trinh, K. Bienkowski, P. Wróbel, M. Pisarek, A. Parzuch, N. Nawaz, *et al.*, "New concept for the facile fabrication of core–shell CuO@ $CuFe_2O_4$ photocathodes for PEC application," *Materials (Basel).*, vol. 15, no. 3, p. 1029, 2022.

[39] A. C. Nawle, A. V Humbe, M. K. Babrekar, S. S. Deshmukh, and K. M. Jadhav, "Deposition, characterization, magnetic and optical properties of Zn doped $CuFe_2O_4$ thin films," *J. Alloys Compd.*, vol. 695, pp. 1573–1582, 2017.

[40] D. Taye, S. Mohanty, A. K. Das, and N. K. Singh, "Electroless Ni–Al_2O_3–WS_2 composite coating on aluminum substrate," *Trans. Indian Inst. Met.*, vol. 72, pp. 2281–2292, 2019.

[41] Y. Wan, X. Wang, H. Sun, Y. Li, K. Zhang, and Y. Wu, "Corrosion behavior of copper at elevated temperature," *Int. J. Electrochem. Sci.*, vol. 7, no. 9, pp. 7902–7914, 2012.